Proceedings of IMECE2006
2006 ASME International Mechanical Engineering Congress and Exposition
November 5-10, 2006, Chicago, Illinois, USA

IMECE2006-13595

DESIGN OF SPRING COUPLING FOR HIGH Q, HIGH FREQUENCY MEMS FILTERS

Mohammed Shalaby
Department of Mechanical Engineering
University of Michigan, Ann Arbor, MI
mshalaby@umich.edu

Mohammed Abdelmoneum
Intel Corporation
Hillsboro, OR
mohamed.a.abdel-moneum@intel.com

Kazuhiro Saitou
Department of Mechanical Engineering
University of Michigan, Ann Arbor, MI
kazu@umich.edu

ABSTRACT

This paper presents the design optimization of the coupling beam of wine glass (WG) mode micromechanical disk filters using the simulated annealing algorithm. The filter under consideration consists of two identical wine-glass mode disk resonators, mechanically coupled by a flexural mode beam. Such coupled two-resonator system exhibits two mechanical resonance modes with closely spaced frequencies that define the filter passband. The frequencies of the constituent resonators determine the center frequency of the filter, while the bandwidth is determined by the stiffness and location of attachment of the coupling beam. The goal is to design a filter with a commonly used bandwidth, namely 100 kHz. The design variables that control the bandwidth value are the beam length, the beam width, and the location of attachment of the coupling beam from the center. The simulated annealing algorithm is used to solve the optimization problem, since the governing dynamic equations of the resonator-coupling system are highly nonlinear. The resulting optimum design is simulated using the finite element method, which confirms the achievement of the desired center frequency and bandwidth.

INTRODUCTION

Frequency selective and generating components namely filters and oscillators are inherent building blocks in any modern wireless transceiver system as they play a key role in determining the overall system performance and sensitivity [1][2]. In today's systems, off-chip mechanically resonant components, such as crystal resonators and filters [3], surface acoustic wave (SAW) filters [4][5], and film bulk acoustic resonators (FBAR's) [6][7], are used to realize high-Q bandpass filters, commonly used in the radio frequency (RF) and intermediate frequency (IF) stages of heterodyne transceivers [4]. These mechanical components have higher quality factors compared to their transistor based counterparts [8][9]; as a result, they greatly outperform comparable filters implemented using transistor technologies [2][4]. On the other hand, these mechanical devices are bulky, and cannot be integrated on chip due to their non CMOS compatible fabrication technology. In addition, the insertion loss associated with these off chip components affect the system performance and reduces the battery life time if additional amplification stages are to be used [8][9]. For these reasons, research on how to implement MEMS based filters and oscillators is currently an active area of research [10][11].

The remainder of this paper is organized as follows. The next section presents the earlier work done related to the context of this paper. Then, the theory behind high-frequency μmechanical resonators design and μmechanical filter design is presented. Simulated annealing is then used to tune the coupling beam dimensions and coupling location to a certain desired bandwidth. Finally, the fabrication process is described.

RELATED WORK

Advances in surface micromachining technologies made it possible to fabricate on-chip high-Q micromechanical resonators and filters [12][13][14]. Vibrating Micro Electro Mechanical (MEMS) Wine Glass mode disk resonators fabricated using poly-silicon as the structural material first demonstrated by Abdelmoneum *et al.* [15][14] exhibited Q's of more than 96,000 under vacuum and 8,600 in atmosphere and center frequency around 71 MHZ [14]. Later, resonators with Q's in the excess of 145,000 in vacuum [16] were incorporated in demonstrating reference oscillators with phase noise performance surpassing GSM requirements. At this point, it appears that micromechanical resonators (abbreviated "μresonators") can potentially serve well as miniaturized substitutes for crystals in a variety of high-Q oscillator and filtering applications.

MF (*eg*., 455 kHz) MEMS filters were demonstrated early in literature [17][18]. Later, higher frequency MEMS filters, with frequencies around 7.8 MHz and percent bandwidths from 0.2% to 2.5% (Q from 40 to 450) were demonstrated by Bannon, *et al.* [19]. Unfortunately, filters at much higher

frequencies are still needed for useful implementation in communication systems in particular at RF range. This work focuses on frequencies in the vicinity of 71 MHz and percent bandwidth from 0.14% to 1.6% (Q 62 to 710) however practical implementation is not limited to this range.

NOMENCLATURE

f_o: resonance frequency
R: disk radius
ρ: material density
σ: Poisson's ratio
E: Young's modulus of elasticity
$\omega_0 = 2\pi f_o$: natural angular frequency
U: radial displacement component
V: tangential displacement component
m_{re}: resonator effective mass
K_{re}: resonator effective stiffness

MICROMECHANICAL RESONATOR

Wine Glass (WG) mode disk resonators

High frequency, stemless wine-glass mode disk resonator has been presented earlier by Abdelmoneum *et al*. [14]. Figure 1a presents the SEM of the wine-glass mode disk resonator. The resonator features four anchored supports attached to the disk at its four wineglass nodal points. This wine-glass resonator is able to operate with substantially high-Q.

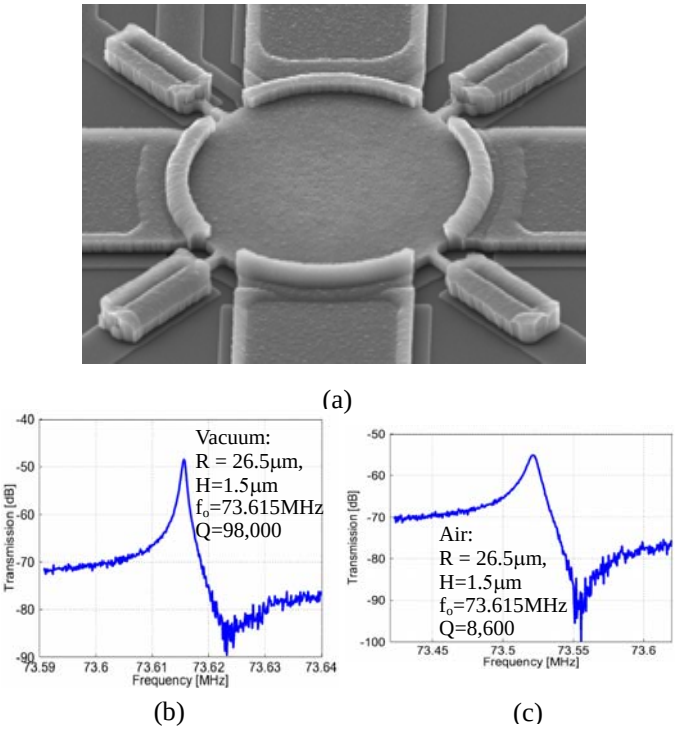

Figure 1: Wine glass mode resonator [14]. (a) SEM picture, measured frequency spectrum in vacuum (b), and in air (c).

The electrodes are located around the circumference of the disk, one in each of the four quadrants about a 1,000Å from the disk and are used for electrostatic excitation and detection. To select the wine-glass mode shape, identical signals should be applied on opposing electrodes along one axis. The sensing can be done using the electrodes on the orthogonal axis; they can also be connected to an out-of-phase input signal to add additional drive force.

Figures 1b and 1c present the measured frequency response for a 73-MHz version measured in vacuum and air respectively. With only two successive perimeter nodal supports, the Q was about 98,000 in vacuum and 8,600 in air. The reasons of such high Q are: 1) the disk supports are at the four nodal points where the displacement is almost zero, so minimum energy is transferred to substrate through anchors, not like clamped beam resonators 2) fabrication error in support location is minimum, because they are done in the same stage the resonator is deposited, not like stemmed wine glass resonators and 3) squeeze film damping effect for this resonator is minimal since the resonator vibrates in plane, and the surface area is very small compared to that of plane clamped beam resonators.

Governing equations

The Wine-Glass mode disk vibrates in an elliptical mode shape as seen in Figure 3. This mode is a compound mode in which the displacement vector consists of two orthogonal components, a tangential component and a radial one. Assuming the disk thickness is much smaller than its radius, the disk can be approximated as a thin circular plate. The mode equation for the lowest order compound mode for a circular plate was derived by Onoe *et al.* [21] where the mode frequency f_o for a wine-glass mode disk can be obtained by solving the mode frequency equation:

$$\left[\Psi_2\left(\frac{\zeta}{\xi}\right)-2-q\right]\left[2\Psi_2(\zeta)-2-q\right]=(nq-n)^2 \qquad (1)$$

where

$$q=\frac{\zeta^2}{2n^2-2},\quad \zeta=R\sqrt{\frac{2\rho\omega_o^2(1+\nu)}{E}},\quad \xi=\sqrt{\frac{2}{1-\nu}} \qquad (2)$$

R is the disk radius, $\omega_o=2\pi f_o$ is the angular frequency, $n=2$ is the mode order, and ρ, ν, and E are the density, Poisson ratio, and Young's modulus, respectively, of the disk structural material.

The effective mass of resonator at any point on the disk periphery can be evaluated with:

$$\frac{1}{2}m_{re}v_{re}^2=KE_{total} \qquad (3)$$

where KE_{total} is the total kinetic energy the resonator obtained by integrating over the resonator volume. The total kinetic

energy is equal to the summation (integration) of the product of an infinitesimal mass and velocity the total velocity of that mass. The computed total kinetic energy is also equal to the product of the effective mass at a specific location m_{re} and the corresponding velocity, v_{re} at the same location. Implementing the wine-glass mode disk resonator equation, the above equation can be rewritten as:

$$m_{re} = \frac{\rho\pi H \int_0^R r\left[\frac{\zeta}{2R\xi}J_1\left(\frac{\zeta r}{\xi R}\right) - \frac{\zeta}{2R\xi}J_3\left(\frac{\zeta r}{\xi R}\right) + \frac{B}{rA}J_2\left(\frac{\zeta r}{R}\right)\right]^2 dr}{\left[\frac{\zeta}{2R\xi}J_1\left(\frac{\zeta r_c}{\xi R}\right) - \frac{\zeta}{2R\xi}J_3\left(\frac{\zeta r_c}{\xi R}\right) + \frac{B}{r_c A}J_2\left(\frac{\zeta r_c}{R}\right)\right]^2} \quad (4)$$

where H is the disk thickness, B/A = -4.5236 and J_n is Bessel function of the first type and order n. Now the effective stiffness at the coupling location can be evaluated with:

$$K_{re} = \omega^2 m_{re} \quad (5)$$

MICROMECHANICAL FILTER

Filter structure and operation

The μmechanical filter considered in this paper consists of two identical mechanical wine-glass mode disk resonators, mechanically coupled by a flexural-mode or an extensional mode beam, all suspended at 4000 Å above the substrate. Capacitive transducer electrode is positioned on the side of one of the resonators to excite the resonator vibration in the desired wine-glass vibration mode. Another electrode is positioned on the side of the other resonator to read the output response from the filter.

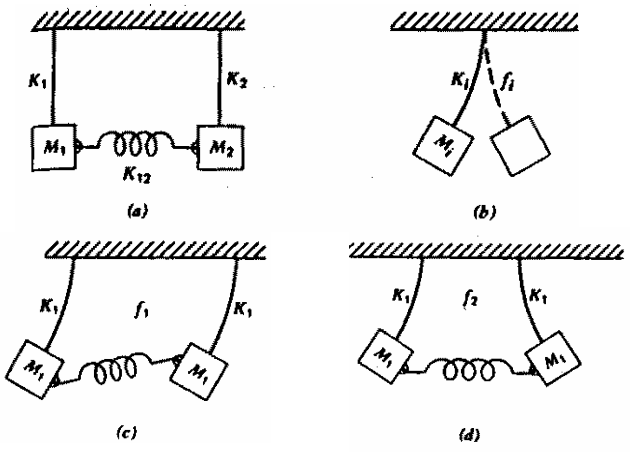

Figure 2: Coupled spring-mass resonators. (a) resonators at rest, (b) single resonator natural mode, (c) in phase mode, (d) out of phase mode [20]

Such a coupled two-resonator system exhibits two mechanical resonance modes with closely spaced frequencies that define the filter passband. Figure 2 shows the equivalent lumped mass mechanical system of the filter. The frequencies of the constituent resonators determine the center frequency of the filter, while the bandwidth is determined by the stiffness of the coupling spring and the coupling location. As shown in Figure 3, each mode peak corresponds to a distinct, physical mode shape. In the lower frequency mode, the resonators are 180° out of phase; and in the higher frequency mode, both resonators vibrate in phase.

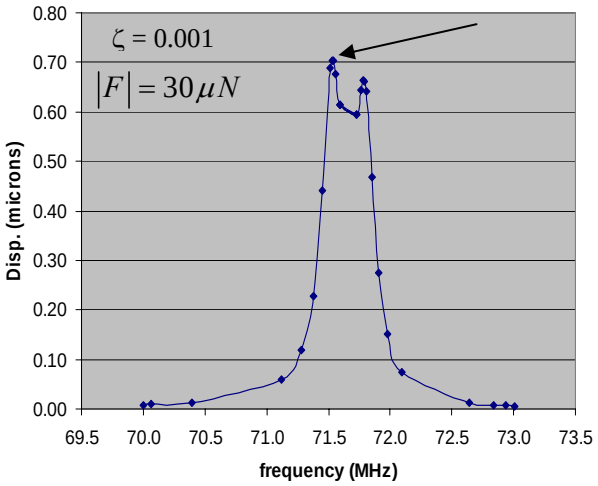

(a)

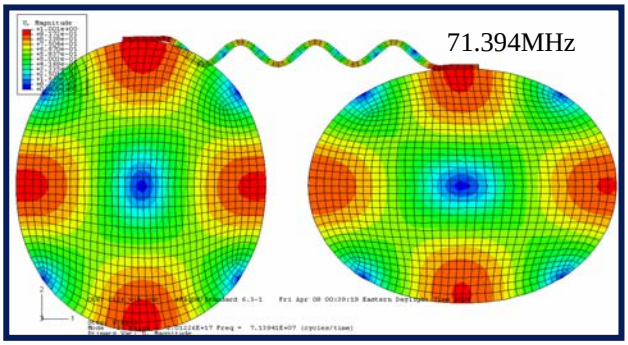

(b)

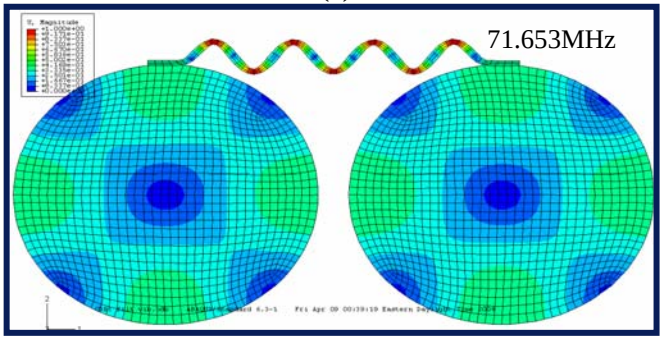

(c)

Figure 3: Simulation for filter flexural mode coupling. (a) un-terminated frequency response plot (b) out of phase mode, and (c) in phase mode

The operation of this filter can be seen as a device that takes an electrical input signal, converts it to mechanical signal, processes this signal in the mechanical domain, then converts the resulting signal once more to an electrical output signal, ready for further processing by subsequent electronic stages.

Governing equations

The filter design is dominantly governed by the bandwidth equation:

$$BW = \frac{f_o}{K_{ij}} \frac{K_c}{K_{re}} \tag{6}$$

where f_o is the center frequency of the filter, its also the resonant frequency of each of the resonators, K_{ij} is the normalized coupling coefficient (K_{ij} = 0.7225 [22]), K_c is the coupling beam stiffness and K_r is the resonator effective stiffness at the coupling location. It is obvious that the bandwidth depends only on the resonator stiffness, *i.e.* the coupling location on the resonators, and the coupling beam stiffness. The other two parameters are constants. In such micro-scale filters, it may not be possible to design a highly compliant coupling beam for desired low bandwidth filters. As a result, the coupling location plays an important role in determining the filter bandwidth as well, as it affects the resonator effective stiffness. As will be shown later, if the coupling is at low velocity location on the resonator, effective mass increases and so is the effective stiffness, consequently, the filter bandwidth decreases.

Extensional mode and torsional mode coupling elements have similar equations. The stiffness of the coupling beam is given by equation 7:

$$K_c = \omega A \sqrt{\rho E} \quad l = \frac{n\lambda}{4} \quad n = 1,3,5,... \tag{7}$$

Due to the fact that in such micro-scale the coupling beam mass and the resonator mass are of the same order. As a result, it is important to account for the coupling beam mass. Since this is not an easy process, an easier way is to set the beam length equal to an odd multiple of quarter the wavelength. As a result, the coupling beam mass should has no effect on the resonator frequency [17][23].

For the flexural mode coupling with clamped ends, the beam stiffness is calculated using equation 8.

$$K_c = \frac{EI\alpha^3\left(\sin\alpha + \sinh\alpha\right)}{L^3\left(\cos\alpha\cosh\alpha - 1\right)}, \qquad \alpha = \sqrt[4]{\frac{\rho A\omega^2}{EI}}L \tag{8}$$

Again it is important to find the coupling beam dimensions that correspond for the quarter wavelength to eliminate the effect of the coupling beam mass. As a result the equality given by equation 9 should be satisfied.

$$H6 = \sin\alpha\cosh\alpha + \cos\alpha\sinh\alpha = 0 \tag{9}$$

Simulations of flexural mode filters

Figure 3 shows the filter's simulated peak frequencies as well as the un-terminated frequency response plot. A manufacturable coupling beam width of 1 μm was chosen, beam stiffness and beam length were obtained from Equation 8. The coupling location was chosen to be at the outer radius of the resonators. Using Equation 3, the bandwidth was 259 kHz.

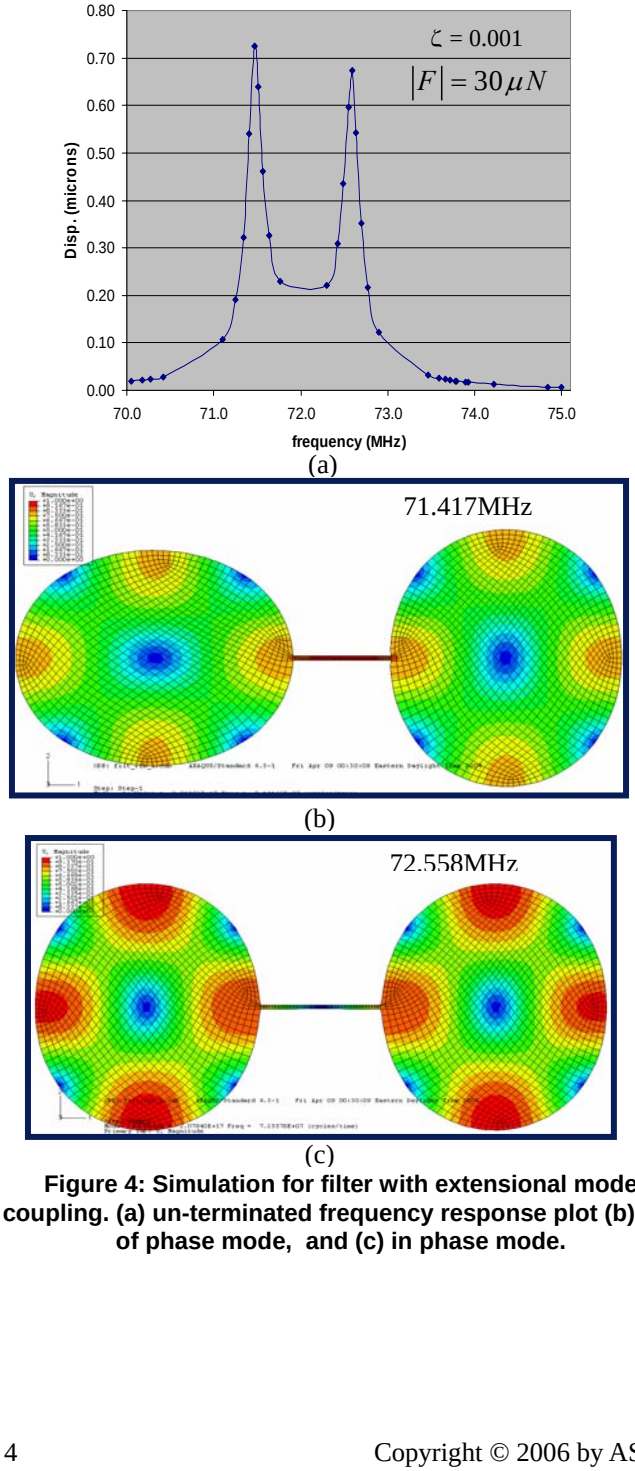

Figure 4: Simulation for filter with extensional mode coupling. (a) un-terminated frequency response plot (b) out of phase mode, and (c) in phase mode.

Simulations of extensional mode filters

Figures 4a and 4b show the filter's simulated peak frequencies, while Figure 3c shows the filter's un-terminated frequency response plot. A manufacturable coupling beam width of 1 μm was chosen, beam stiffness and beam length were obtained from Equation 7. The coupling location was chosen to be at the outer radius of the resonators. Using Equation 3, the BW is 1.14 MHz.

OPTIMIZATION OF μMECHANICAL FILTER FOR A DESIRED BANDWIDTH

It is clear that the bandwidth for the extensional mode coupling is much larger than that for the flexural mode coupling. This is due to the fact that the beam stiffness in extensional mode is much higher than its stiffness in flexural mode. In conclusion, if the desired bandwidth is in the range of hundreds of kHz, flexural mode coupling beams need to be used. While for bandwidths in the order of MHz extensional mode coupling beams need to be used.

Since filters are designed to have a certain bandwidth at a certain given frequency, at this stage, the objective is to find a WG mode filter that has a bandwidth of 100 kHz. Optimization is used to reach the desired target bandwidth.

Definition of design variables

It can be deduced from equation 6 that the bandwidth depends on the resonator stiffness and the coupling beam stiffness. Equations 4 and 5 show that the resonator stiffness can be controlled by controlling the resonator thickness, H, and the coupling location, r_c. While, from equations 7 and 8, the coupling beam stiffness is controlled by the coupling beam dimensions (length, width and thickness).

Since the thicknesses of the beam and the resonator are controlled by the manufacturing process, they are not selected as design variables. As a result, the design variables, selected, are the beam length (l), the beam width (w) and the coupling location from the center (r_c).

Definition of constraints

The upper and lower bounds over the beam width are again governed by the manufacturing process. Since the coupling location has to be off the disk center and along the vertical direction to transfer all the vertical energy, without any horizontal energy component, the beam length has to be at least equal to the disk diameter. In addition, if the beam length exceeds a certain value, equations 7 and 8 gets unsolvable because of their extreme nonlinearity. Consequently, the upper and lower bounds over the beam length are obtained. The upper bound over the coupling location is simply the beam radius. In addition, two more equality constraints are needed to ensure that the resulting bandwidth is equal to 100 KHz, and that equation 9 is satisfied. Mathematically, these constraints can be written as:

$$0.75 \le w \le 2.0\mu m \tag{10}$$

$$55 \le l \le 90\mu m \tag{11}$$

$$10 \le r_c \le 26.5\mu m \tag{12}$$

$$h_1 = abs\left(BW - 100\times10^3\right) = 0 \tag{13}$$

$$h_2 = H6 = 0 \tag{14}$$

Definition of design objective

Since the objective here is to reach a certain bandwidth can be easily handled as a constraint, as shown earlier. And since the satisfaction of the second equality constraint (h_2) is too hard due to the high nonlinearity of the equation, the authors considered minimizing the absolute value of $H6$ as a design objective, as shown in equation 15. This way $H6$ can get as close to possible to zero, as needed, without really affecting the actual problem. As a result, h_2 is no longer considered as a constraint and removed from constraints equations, given earlier.

$$\min\left(abs\left(H6\right)\right) \tag{15}$$

Optimization method

Simulated annealing [24][25], first introduced by Kirkpatrick *et al.* [24], is a global stochastic optimization method capable of finding optimal or near-optimal solutions to problems with ill-behaved objective functions which resist optimization by traditional gradient-based techniques. Simulated annealing has a broad range of use in realistic engineering problems because they are often characterized by poorly behaved objective functions [26].

The high nonlinearity in the objective function and the constraints, in the current optimization problem, prevented normal gradient based algorithms, such as sequential quadratic programming (SQP) [27] from performing well. As a result, simulated annealing was used and it was able to reach a near optimal solution. The detailed algorithm was earlier written in [28].

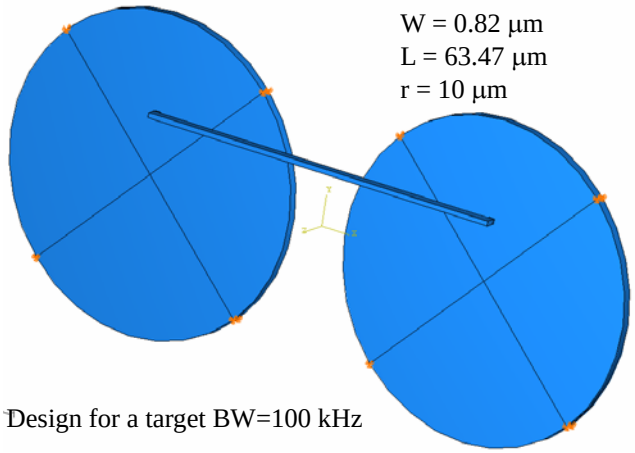

Figure 5: 3D model of the proposed 100 kHz bandwidth filter

The optimum values of the design variables are l = 63.47 mm, w = 0.82 mm and r_c = 10 mm. A 3D model for the filter is shown in Figure 5. Figures 6a and 6b show the filter's simulated peak frequencies, while Figure 6c shows the filter's un-terminated frequency response plot.

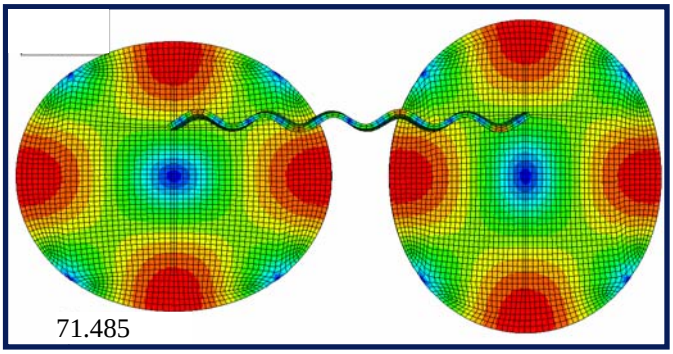

(a)

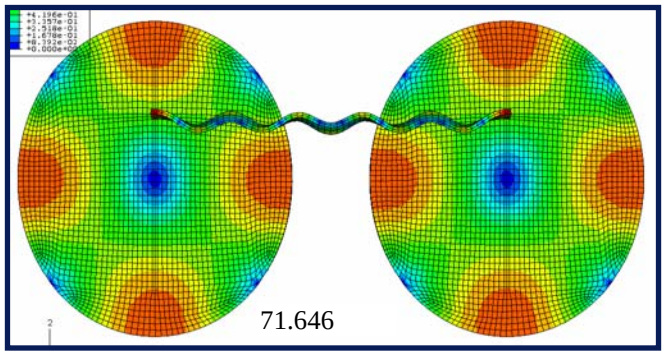

(b)

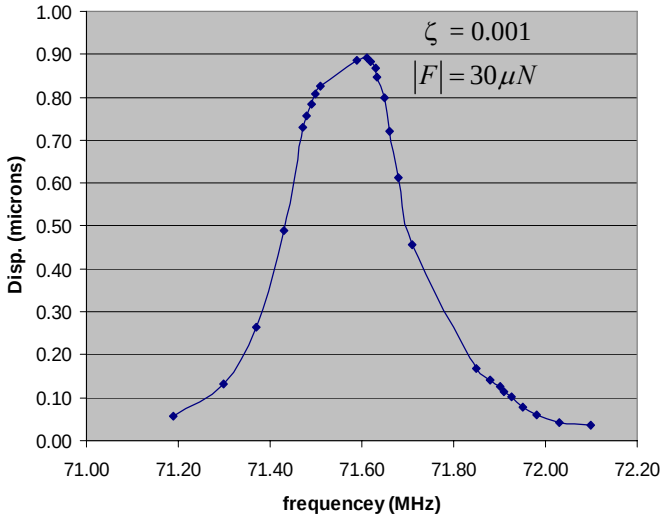

(c)

Figure 6: Simulation for filter with 100 kHz bandwidth. (a) out of phase mode, (b) in phase mode, (c) un-terminated frequency response plot

FABRICATION AND LAYOUT

The first demonstrated Wine-Glass mode disk resonator was fabricated using a self aligned surface micromachining process that uses poly silicon as the structural material [14]. This self aligned process eliminates Q degradation resulting from anchor losses that take place due to anchor misalignment (during the anchor patterning step) to the mode nodal points [29]. The selection of the disk structural material is not limited to poly silicon only, higher frequencies can be achieved by using materials with higher modulus of elasticity like diamond and silicon carbide [15]. The proposed filter can be fabricated using the same self aligned processes used to fabricate the first Wine-Glass mode resonator [14].

Figure 7 shows a 3-D schematic of the first demonstrated Wine-Glass mode disk resonator [14]. The device consists of three poly silicon layers. The first layer is a 3000 A^o thick layer that defines the input/output and bias interconnects. The second layer is a 2μm structural layer that simultaneously defines the disk structure and anchor openings (self aligned layer). The third layer is a 2μm layer that refills the anchor openings and make contact to the interconnect layer and defines the input/output electrodes.

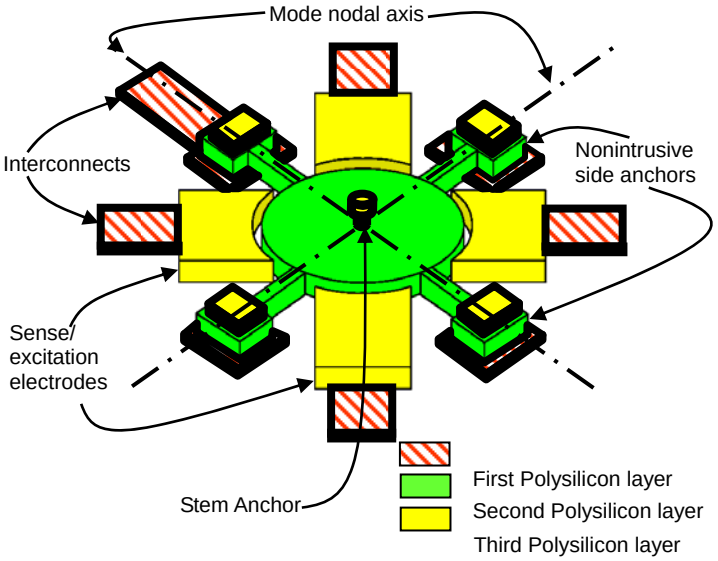

Figure 7: A schematic for the Wine-Glass mode disk fabricated using the self aligned process

The process starts by forming a passivation layer on top of a bare silicon substrate. The paasivation layer is formed of a 2 μm thick oxide layer followed by the deposition of 0.3 μm Nitride layer both deposited in the same furnace using low pressure chemical vapor deposition (LPCVD). Following the deposition of the passivation layers, a 3000 Å poly silicon layer is then deposited using LPCVD, doped using POCL doping and patterned using reactive ion etching (RIE). This silicon layer serves as the "interconnects" layer (first poly silicon layer shown in Figure 7) which provides input/output/bias lines to the device. To isolate the structural poly silicon layer (second

poly layer shown in Figure 7) to be deposited later from the formed interconnect poly layer, a 0.5 μm oxide layer is deposited using LPCVD. A 2 μm structural poly layer is then deposited using LPCVD, doped using POCL doping and then followed by depositing a 0.5 μm oxide hard mask layer. The top oxide hard mask is then patterned to form the mask for the disk structure and the anchors. This pattern is then transferred to the underlying structural poly layer using RIE. This is the self aligned step in which both of the disk structure and the anchors are defined in the same patterning step thus eliminating any misalignment between the anchor and the mode nodal points.

The capacitive gap separating the disk structure from the electrodes (to be deposited and patterned) is then defined by depositing a 1000 Å of oxide. This thin oxide layer will be etched away during the release step to form the capacitive air gap. It should be noted that other high dielectric materials (high K) can be deposited instead of oxide. The use of high K materials to form the capacitive gap is interesting as it can substantially reduce the motional resistance of the resonator and hence alleviate impedance matching problems. However, the problem lies in processing these materials with enough selectivity compared to silicon oxide so that they are not etched away with the sacrificial oxide during the final release step.

Anchor and electrode openings are then patterned and etched through the spacer oxide and the sacrificial oxide layers to provide direct electrical contact between the interconnects poly silicon layer and the anchor/electrode layer to be deposited next. The third and last 2 μm poly silicon layer forming anchor and electrodes are then deposited using LPCVD, doped using POCL doping and caped with 0.5 μm of hard mask oxide deposited using LPCVD. The deposited poly layer refills the anchor openings and make both electrical and mechanical contacts to the interconnect poly layer. The pattern on the top oxide hard mask is then transferred to the underlying third poll are via RIE to form the input output electrodes and anchors. Finally the device is released using HF and dried using super critical cleaning.

CONCLUSION

The paper presented the modeling and optimization of the wine-glass mode disk resonator for high frequency (about 71 MHz) high *Q* filters with bandwidths of 100 kHz. Such filters can find their way to replace bulky and off chip crystal and SAW high-*Q* bandpass filters, commonly used in the radio frequency (RF) and intermediate frequency (IF) stages of heterodyning transceivers. Simulated annealing was used to find the coupling location and the coupling beam dimensions to obtain a desired filter bandwidth. The algorithm was implemented to design a filter with bandwidth of 100 kHz as an example. The algorithm can be implemented to any other desired bandwidths as well.

Upon the experimentation of the equations governing the bandwidth, it can be deduced that the design is mostly sensitive to slight tolerances in the beam width. This is because the current fabrication techniques have no accurate control on such dimension. The variation in the beam width can be around 0.2 μm. With a width of 0.82 mm, the tolerance is 24%. This means that at least the bandwidth will vary by 24% as well. Also a variation in the beam width will violate equation 9 for flexural mode beam coupling, and so the filter center frequency may be affected. Since there are no analytical equations model the effect of the coupling beam mass on the filter center frequency, tedious finite element simulations would be needed to do complete sensitivity analysis for the designed filter.

Finally, the fabrication process is similar to regular MUMPS process. The only slight variation is that it needs the creation a nano gap between the electrodes and the resonator disks. This is done by depositing a very thin sacrificial oxide layer (OX2) of 0.1 μm thickness.

ACKNOWLEDGMENTS

This paper was done as a part MEMS course instructed by Prof. Katsuo Kurabayashi, department of Mechanical Engineering, University of Michigan.

REFERENCES

[1] A. B. Carlson, *Communication Systems*, Electrical and Electronic Engineering Series, McGraw-Hill International Editions, ISBN 0-07-100560-9.

[2] B. Razavi, *RF Microelctronics,* Prentice Hall Communications Engineering and Emerging Technologies Series, ISBN 0-13-8875715.

[3] R. G. Kinsman, *Crystal Filters*, John Wiley and Sons, ISBN 0-471-88478-2.

[4] S. K. Mitra and C. F. Kurth, *Miniaturized and Integrated Filters*, John Wiley and Sons, ISBN 0-471-84496-9.

[5] S. Datta, *Surface Acoustic Wave Devices*, Prentice-Hall, Englewood Cliffs, ISBN 0-13-877911-2.

[6] S. V. Krishnaswamy, J. R. Rosenbaum, S. S. Horwitz and R. A. Moore, 1992, "Film bulk acoustic wave resonator and filter technology," *Technical Digest of the IEEE MTT-S*, pp. 153-155.

[7] R. C. Ruby, P. Bradley, Y. Oshmyansky, and A. Chein, 2001, "Thin film bulk wave acoustic resonators (FBAR) for wireless applications," *Technical Digest of the IEEE Ultrasonics Sumposium*, pp. 813-821.

[8] C. T.-C Nguyen, 1999, "Microelectromechanical components for miniaturized low-power communications*," IEEE MTT-S,* Anaheim, California, pp. 48-77.

[9] C. T.-C Nguyen, 2000, "Microelectromechanical circuits for communications transceivers," Proceedings of the *Bipolar/BiCMOS Circuits and Technology Meeting (BCTM),* Minneapolis, Minnesota, pp. 25-26.

[10] P. Reddy and S. Ravi, 2004, "GA-tuned microelectromechanical filters for signal processing," *Proceedings of the 7th International Conference on Signal Processing ICSP '04*, pp.384 - 387 vol.1.

[11] S.-S. Li, Y-W. Lin, Z. Ren, and C.T.C. Nguyen, 2005, "Self-switching vibrating micromechanical filter bank," Proceedings of the *IEEE International Frequency Control Symposium and Exposition,* pp. 29-31.

[12] R. T. Howe and R. S. Muller, 1986, "Resonant microbridge vapor sensor," *IEEE Trans. on Electron Devices*, vol. 33, no. 4, pp. 499-506.

[13] W. C. Tang, T.-C. H. Nguyen and R. T. Howe, 1989, "Laterally driven polysilicon resonant microstructures," *Sensors Actuators*, vol. 20, pp.~25--32.

[14] M. Abdelmoneum, M. Demirci, and C. Nguyen, 2003, "Stemless Wine-Glass-Mode disk micromechanical resonators," Proceedings of the *IEEE Sixteenth Annual International Conference on Micro Electro Mechanical Systems*, Kyoto, Japan, January 19-23, pp. 698-701.

[15] "*Stemless Wine Glass Mode Disk Resonators*" United States Patent Office 333 199 000, International Patent H03H009/24.

[16] Y-W Lin, S. Lee, S-S Li, Y. Xie, Z. Ren and C. Nguyen, 2004, "Series-resonant VHF micromechanical resonator reference oscillators," *IEEE Journal of Solid State Circuits*, Vol. 39, No. 12, pp.2477-2491.

[17] K. Wang, F. Bannon, J. Clark, and C. Nguyen, 1997, "Q-enhancement of microelectromechanical filters via low velocity spring coupling," Proceedings of the *IEEE International UltraSonics Symposium*, Toronto, Canada, October 5-8, pp. 323-327

[18] F. Bannon, J. Clark and C. Nguyen, 2000, "High-Q HF microelectromechanical filters," *IEEE Journal of Solid-State Circuits*, Vol. 35, pp 512-526.

[19] D. Greywall and P. Busch, 2002, "Coupled micromechanical drumhead resonators with practical applications as electromechanical bandpass filters," *Journal of Micromechanics and Microengineering*, Vol. 12, pp. 925-938.

[20] R. Johnson, 1987, *Mechanical Filters in Electronics,* New York, NY, Wiley.

[21] M. Onoe, 1956, "Contour vibrations of isotropic circular plates," *Journal of Acoustical Society of America*, Vol. 28, pp. 1158-1162.

[22] A. Zverev, 1967, *Handbook of Filter Synthesis*, New York, Wiley.

[23] K. Wang and C. Nguyen, 1997, "High-order micromechanical electronic filters," Proceedings of the *10th Annual International Workshop on Micro Electro Mechanical Systems,* Nagoya, Japan, January 26-30, pp. 25-30.

[24] S. Kirkpatrick, C.D. Gellat, and M.P. Vecchi, 1983, "Optimization by simulated annealing," *Science*, Vol. 220, pp. 671-680.

[25] P. Laarhoven, and E. Aarts, 1987, *Simulated Annealing: Theory and Applications*, D. Reidel Publishing Company.

[26] S. Szykman, L. Schmidt, and H. Shetty, 1997, "Improving the efficiency of simulated annealing optimization through detection of productive search," Proceedings of ASME Design Engineering Technical Conferences and Computers and Information in Engineering Conference, Sacramento, California, September 14-17, Paper No. DETC97/DAC-3980.

[27] S.S. Rao, 1999, *Engineering Optimization, Theory and Practice,* Third Edition, John Wiley and Sons, Inc.

[28] M. Shalaby, 2002, "Topology optimization of structures using hybrid simulated annealing," M.Sc. Thesis, Mechanical Design and Production Department, Cairo University.

[29] J. Clark, W-T Hsu, M. Abdelmoneum and C. T.-C. Nguyen, "High-Q UHF micromechanical radial-contour mode disk resonators," *IEEE Journal of Microelectromechanical Systems,* Vol. 14, NO. 6, Dec. 05, pp. 1298-1310.

APPENDIX: STEP-BY-STEP FABRICATION FIGURES

1. 0.6 μm LPCVD nitride

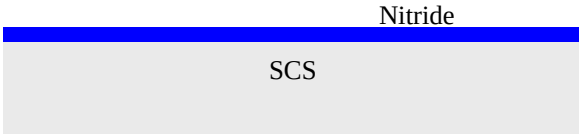

2. 1.3 μm LPCVD Oxide1 / C1S

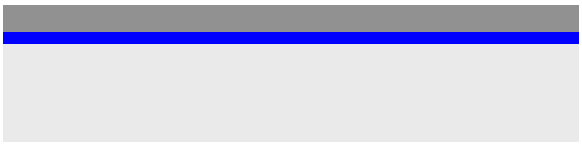

3. 1.5 μm LPCVD PolySi / POLY1

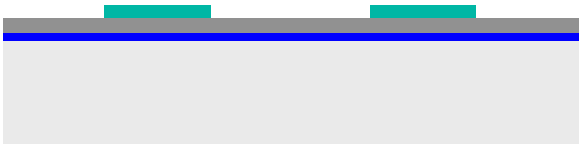

4. 0.1 μm LPCVD Oxide2 / C2S / C21

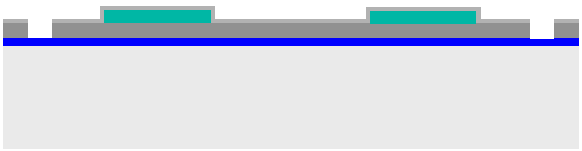

5. 1.5μm LPCVD PolySi + doping / POLY2
6. HF + Release